CHIN. PHYS. LETT. Vol. 38, No. 5 (2021) 057306

Level Statistics Crossover of Chiral Surface States in a Three-Dimensional Quantum Hall System

Rubah Kausar[1], Chao Zheng(郑超)[1*], and Xin Wan(万歆)[1,2]

[1]*Zhejiang Institute of Modern Physics, Zhejiang University, Hangzhou 310027, China*
[2]*CAS Center for Excellence in Topological Quantum Computation, University of Chinese Academy of Sciences, Beijing 100190, China*

(Received 29 December 2020; accepted 15 March 2021; published online 2 May 2021)

Recent experiments have demonstrated the realization of the three-dimensional quantum Hall effect in highly anisotropic crystalline materials, such as $ZrTe_5$ and $BaMnSb_2$. Such a system supports chiral surface states in the presence of a strong magnetic field, which exhibit a one-dimensional metal-insulator crossover due to suppression of surface diffusion by disorder potential. We study the nontrivial surface states in a lattice model and find a wide crossover of the level-spacing distribution through a semi-Poisson distribution. We also discover a nonmonotonic evolution of the level statistics due to the disorder-induced mixture of surface and bulk states.

DOI: 10.1088/0256-307X/38/5/057306

The quantum Hall effect (QHE) in two-dimensional (2D) electron systems arises from discrete Landau levels forming in a strong magnetic field.[1,2] Usually, the QHE is considered to be specific to two dimensions because the band dispersion along the magnetic field generally closes the quantum Hall (QH) gap in three-dimensional (3D) systems. However, the QHE will survive if the hopping strength along the magnetic field is much smaller than the Landau level spacing.[3,4] This idea was first realized in an engineered semiconductor multilayer system,[3,5] and very recently was realized in an anisotropic layered material $BaMnSb_2$.[6,7] There are also other schemes to realize the QHE in 3D, such as by formation of charge density wave under a strong magnetic field.[8−13] The 3D QHE has drawn increasing attention recently due to its experimental realization in anisotropic layered materials.[14−20]

Disorder plays a crucial role in the observation of the Hall plateau. In the 2D QHE, all states are localized except at a critical energy at or near the center of each Landau band, where the QH plateau transitions take place.[21] In the 3D case, the extended states broaden into a metallic band due to the weak coupling between layers.[4,22] As a result, 3D QH systems feature a metallic phase, an insulating phase, and a QH insulating phase in the bulk. Meanwhile, 2D QH systems host chiral edge states inside the QH gap, which are robust against disorder due to their topological nature. In 3D, the chiral edge states of each layer are coupled to its adjacent layers, forming a 2D chiral surface state.[23] Interestingly, in a mesoscopic sample the chiral surface states exhibit three distinct transport regimes, corresponding to a 2D chiral metal, a quasi-one-dimensional (1D) metal, and a quasi-1D insulator along the magnetic field.[24−29]

The standard model for the 3D QHE is the Chalker–Coddington network model,[4,26−31] which describes the percolation of electrons in a slowly varying disorder potential and a strong magnetic field.[32,33] The model works well in the weak disorder or strong magnetic limits, when the inter-Landau level scattering can be neglected. An alternative model features a tight-binding lattice with on-site disorder, whose Thouless conductance calculation[34] and transfer-matrix study[22] have been reported.

The 3D QH system is of great interest due to the rich phases or regimes of the bulk and surface states, which intertwine in the presence of a moderate disorder. In this regime, one can study the metal-insulator transitions in the bulk, the metal-insulator crossovers on the surface, as well as the dimension crossover in eigenstates in a QH mobility gap with open boundary conditions. The statistics of the energy levels are a versatile tool to study the various crossovers and transitions.[35−40] In the metallic regime, the wave functions are extended and have significant overlaps, leading to strong repulsions among the corresponding energy levels. The random-matrix theory[41] predicts that the nearest-neighbor level statistics follows the Gaussian unitary ensemble (GUE) because the magnetic field breaks the time-reversal symmetry in the system. In the insulating regime, the energy levels become uncorrelated, and the distribution of the energy level spacings follows the Poisson statistics.

In this work, we focus on the level statistics of surface states of the 3D QH insulator in the disordered tight-binding model. While the distribution

Supported by the National Natural Science Foundation of China (Grant No. 11674282), and the Strategic Priority Research Program of Chinese Academy of Sciences (Grant No. XDB28000000).
*Corresponding author. Email: zhengchaonju@gmail.com
© 2021 Chinese Physical Society and IOP Publishing Ltd

of energy-level spacings for bulk states allows us to distinguish the phases, the distribution for the surface states in bulk gaps reveals a wide crossover from a quasi-1D metallic regime to a quasi-1D insulating regime. The level statistics crossover can be quantified by Kullback–Leibler (KL) divergence, which varies monotonically as the localization length varies. We exploit the inverse participation ratio (IPR) to identify and to characterize the surface states in the quasi-1D regimes, which feature chiral surface electrons diffusing along the magnetic field in the presence of surface disorder. In the intermediate disorder range, the mixture of surface states and localized bulk states reduces level correlation before the level statistics flows to the metallic limit.

Model and Bulk Phases. A lattice model for the 3D QHE can be constructed by stacking 2D QHE systems with a magnetic field B along the z direction and with different disorder realizations.[22,34,42] On the αth layer, electrons hop to their nearest neighbors according to the following tight-binding Hamiltonian

$$H_\alpha = -\sum_{\langle ij\rangle}(e^{i\theta_{ij}}c^\dagger_{i,\alpha}c_{j,\alpha}+\text{H.c.})+\sum_i \epsilon_{i,\alpha}c^\dagger_{i,\alpha}c_{i,\alpha}, \quad (1)$$

in which we choose the Landau gauge $\vec{A}=(0,Bx,0)$ and on-site disorder potential $\epsilon_{i,\alpha}$ uniformly distributed in the range $[-W/2,W/2]$. Across the layers, we introduce a weak hopping with strength $t_z \ll 1$ such that the gaps between bands are not closed by the dispersion along the z direction. The full Hamiltonian is thus

$$H=\sum_\alpha H_\alpha - t_z\sum_{i,\alpha}(c^\dagger_{i,\alpha}c_{i,\alpha+1}+\text{H.c.}). \quad (2)$$

The number of bands and their Chern indices depends on the magnetic flux ϕ, in units of the flux quantum $\phi_0 = hc/e$, per unit cell

$$\frac{\phi}{\phi_0}=\frac{Ba^2}{hc/e}=\frac{1}{2\pi}\sum\theta_{ij}. \quad (3)$$

In the following discussion, we fix $\phi=\phi_0/3$ such that we have three bands with Chern number 1, -2, 1 per layer.

The density of states of a $24\times24\times24$ system with periodic boundary conditions is shown in Fig. 1(a) for $t_z=0.1$ and $W=3.0$. Unlike its 2D counterpart, each band contains a range of metallic states in the center with tails of Anderson localized states.[4,22] Characteristic features are well developed in the distribution of nearest-neighbor energy level spacings. Figure 1(b) compares the level statistics near $E=-3.65$ and near $E=-2.80$, in the tail and at the center of the lowest band, respectively. As is expected, the two sets of data agree very well with the Poisson distribution $P(s)=e^{-s}$ and with the GUE distribution

$$\mathcal{P}(s)=\frac{32}{\pi^2}s^2\exp\Big(-\frac{4}{\pi}s^2\Big), \quad (4)$$

which confirms that the system has localized eigenstates in the band tail and metallic states in the band center.

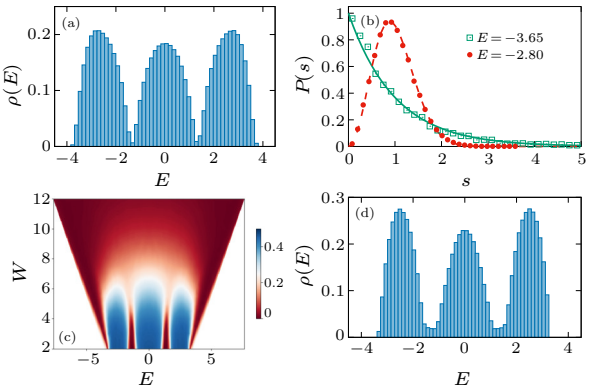

Fig. 1. (a) Density of states of a $24\times24\times24$ cubic lattice for $W=3.0$ and $t_z=0.1$ with periodic boundary conditions. (b) Nearest-neighboring level spacing distribution in the system at energy $E=-3.65$ and -2.80 in the lowest band. Distribution evolves from Poisson to GUE as the energy moves from the band tail to the band center. (c) KL divergence of the nearest-neighboring level spacing in the cubic lattice for $t_z=0.1$ for various W and E. The Poisson distribution is chosen as the reference. (d) Density of states of the cubic lattice for $W=2.0$ and $t_z=0.1$ with open boundary conditions in the xy plane.

To quantify the distribution evolution, we introduce the KL divergence, which is widely used in information theory and machine learning to measure the distance between two distributions. The KL divergence is defined as

$$D_{\text{KL}}[\mathcal{P}'(s)||\mathcal{Q}(s)]=\int ds\mathcal{P}'(s)\log\frac{\mathcal{P}'(s)}{\mathcal{Q}(s)}, \quad (5)$$

where $\mathcal{Q}$ is a reference distribution to which we measure the distance of the distribution $\mathcal{P}'$. In this study, we choose the Poisson distribution as the reference $\mathcal{Q}$ because the vanishing density of states in the band gaps would, otherwise, lead to large fluctuations. When we choose $\mathcal{P}'$ to be the GUE distribution, Eq. (5) yields a KL divergence 0.471. Notice that D_{KL} is not symmetric in $\mathcal{P}'$ and $\mathcal{Q}$.

For the energy-level distribution near $E=-2.80$, we find $D_{\text{KL}}=0.460$, close to that of the GUE distribution. Meanwhile, we find the distribution at $E=-3.65$ has a much smaller distance to Poisson, $D_{\text{KL}}=0.019$. The observation implies that D_{KL} can be applied to visualize the phase diagram of the model. For this purpose, we use exact diagonalization to generate energy levels of 300 samples of size $24\times24\times24$ from $W=2.0$ to 12.0. In Fig. 1(c) we plot the KL divergence of the nearest-neighbor level spacing distribution with increasing disorder. Comparing with the phase diagram obtained by a localization-length calculation,[22] we find that typical localized states, characterized by Poisson level statistics, can be found in regions in dark red with vanishing D_{KL}. Meanwhile, metallic states, characterized by GUE level statistics,

appear in regions in blue, white, and orange, where $D_{\rm KL}$ is significantly greater than zero.

The $D_{\rm KL}$ plot exemplifies how one can map out phase diagrams in the study of a metal-insulator transition. As indicated by the color map, the three Landau bands broaden with increasing W. Metallic states merge into a continuous region of conducting states, while the 3D QHE regimes in between the bands shrink and disappear around $W \approx 4$. Eventually, localization dominates at all energies roughly at $W \gtrsim 10$.

Surface States. The 3D QH insulating phase manifests unusual surface properties when we apply open boundary conditions in x and y directions, while keeping periodic boundary conditions along z direction. In particular, a finite density of states emerges in the bulk band gaps, as shown in Fig. 1(d) for $W = 2.0$ and $t_z = 0.1$. These states are the chiral surface states, which live on the sidewalls of the sample.[4,23] In the presence of disorder, the chiral motion of electrons around the sample suppresses the localization effect along the magnetic field. To make quantum interference happen, an electron has to circumnavigate the sample at least once. If the electron diffuses out of the sample without a complete round-trip, the system is in the so-called 2D chiral metal regime.[24–29] For sufficiently long samples, the interference can happen many times so that the surface states can still be localized. Quantitatively, one finds the surface localization length to be[34]

$$\xi \approx \xi_0 \frac{t_z^2}{W^2} C, \tag{6}$$

where C is the circumference in the xy plane and ξ_0 is found numerically to be 53.2. We note that Eq. (6) is only valid for small t_z and W. For sufficiently large t_z and W, the mobility gaps close, thus the quantum Hall phase and its well-defined surface states no longer exist. When $L_z \ll \xi$, the surface is a quasi-1D conductor, even though the bulk is insulating. For $L_z \gg \xi$, the surface becomes a quasi-1D insulator. To avoid entering the ballistic regime, the 2D chiral metal regime is difficult to approach in an exact diagonalization study.[34] Therefore, we focus on the quasi-1D regime in the following.

We begin by calculating the inverse participation ratio (IPR)

$$\text{IPR} = \sum_{\text{x,y,z}} |\psi(x,y,z)|^4 \tag{7}$$

of the normalized wave functions ψ in a $21 \times 21 \times 21$ system. Roughly speaking, the participation ratio $r = 1/\text{IPR}$ measures the number of sites that a wave function has significant weight. To separate the contribution from the bulk and the surface, we further define the surface IPR of a state as

$$\text{SIPR} = \sum_{\text{surface}} |\psi(x,y,z)|^4, \tag{8}$$

such that the surface-to-bulk ratio $r_{\rm s} = \text{SIPR}/\text{IPR}$ indicates whether the state is a bulk one or 2D-like on the surface. In particular, a pure surface (bulk) state has $r_{\rm s} = 1$ ($r_{\rm s} = 0$).

First, we choose $t_z = 0.2$ and $W = 1.3$ such that we estimate $\xi \approx 106 > L_z$ and, therefore, the surface is a quasi-1D metal. We plot, in one disorder realization, the surface-to-bulk ratio $r_{\rm s}$ against E in Fig. 2(a). We note the percentage of surface sites is $2L_z(L_x + L_y - 2)/(L_x L_y L_z) \approx 18\%$ for $L_x = L_y = 21$. Unsurprisingly, more than 70% of the states have $r_{\rm s} < 0.18$, or have less surface-state occupation than the average value. Meanwhile, Fig. 2(a) shows that $r_{\rm s}$ exceeds 0.95 for $1.12 < |E| < 1.53$, which is consistent with the location of the bulk energy gaps. Clearly, the energy range contains surface states only. To further check whether these surface states are extended or localized in the z direction, we plot $r_{\rm s}$ against the participation ratio r in Fig. 2(b). As indicated in Fig. 2(b), the states with $r_{\rm s} > 0.95$ have r greater than 824, which is about half the number of the surface sites. This confirms that the surface states are metallic with extended wave functions.

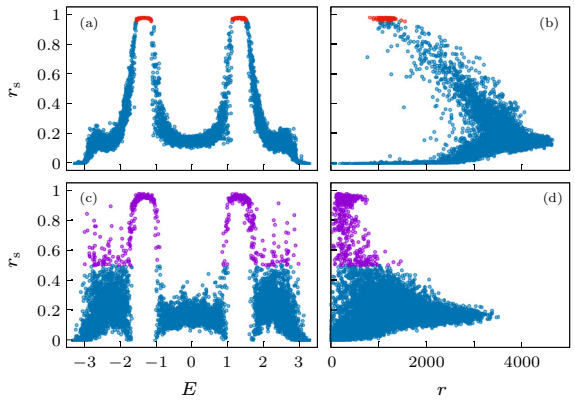

Fig. 2. The surface-to-bulk $r_{\rm s}$ as a function of (a) E and (b) $r = 1/\text{IPR}$ in an arbitrary disorder realization with $t_z = 0.2$ and $W = 1.3$, for which the surface is a quasi-1D metal. The points with $r_{\rm s} > 0.95$ are marked in red. The dependence of $r_{\rm s}$ on (c) E and (d) r in an arbitrary disorder realization with $t_z = 0.04$ and $W = 2.0$, for which the surface is a quasi-1D insulator. The points with $r_{\rm s} > 0.5$ are marked in purple. In both the cases, $L_x = L_y = L_z = 21$.

Next, we consider the surface in the quasi-1D insulator regime, which can be achieved by decreasing t_z and increasing W. We choose $t_z = 0.04$ and $W = 2.0$ such that we estimate $\xi \approx 1.8 \ll L_z$ and, therefore, the surface states are deep in the quasi-1D insulator regime. Figure 2(c) shows that the in-gap states still have $r_{\rm s} \simeq 1$ and are surface states. However, states in the middle of the two side bands occasionally can have $r_{\rm s}$ as large as 0.8. In fact, the side bands have a very broad range of $r_{\rm s}$, indicating that the scattering of surface electrons to the bulk is now strong, leading to wave functions localized near, but not entirely, on the surface. In the central band, however, the mixture

is not as significant, presumably due to the longer localization length of the bulk states.[21] As shown in Fig. 2(d), the average r of the states with $r_s > 0.5$ is only 394, less than a quarter of the surface sites. These observations clearly support that the surface states are insulating in the z direction. In fact, the number can be estimated by assuming that a typical wave function decays exponentially in z axis while having uniform density on the edge in the perpendicular direction. Explicitly, we propose to understand the quasi-1D insulating states with an ansatz surface density

$$|\psi(x,y,z)|^2 = \delta_{x,1}\delta_{x,L_x}\delta_{y,1}\delta_{y,L_y}e^{-2|z-z_0|/\xi}. \quad (9)$$

The IPR of the state can be evaluated to be $(2\xi C)^{-1}$, or $r \approx 300$, closed to the numerical observation. This ansatz, however, has not taken into account density fluctuations, which lead to the fluctuations of the IPR.

The comparison of the IPR in the quasi-1D metallic and quasi-1D insulating regimes is consistent with the picture of the QH phase that a surface electron circles around the sample while diffusing along the magnetic field direction with a characteristic localization length ξ. The 3D QHE system with surface states, therefore, provides an interesting arena to study the quasi-1D metal-insulator crossover of level statistics. For cubic samples, one expects that the level statistics depends on $L/\xi \approx W^2/(4\xi_0 t_z^2)$, which is independent of the system size, according to Eq. (6). In this sense, the surface electrons are in a critical state because the localization length is linearly proportional to the system size itself.[4,29] In the following, we will compare results for cubic systems with $L = 12$ and 18.

We choose the eigenstates with $1.12 < |E| < 1.53$, which has been identified as the range of surface states in the IPR analysis above. Figure 3(a) plots the surface-state level statistics for $t_z = 0.2$ and $W = 1.3$, i.e., $L/\xi = 0.1985$, deep in the metallic regime. Regardless of the system size, the nearest-neighbor level spacings obey the GUE distribution, confirming the metallic nature of the surface states. Figure 3(b) shows that the level statistics for $t_z = 0.01$ and $W = 2.0$, or $L/\xi = 188.0$, follows the Poisson distribution, which indicates the surface states are localized along the z direction. There are, however, some finite-size deviations at small level spacing, due to the repulsion between neighboring states that cannot be located further away. In the crossover regime, the level statistics varies smoothly with L/ξ from the GUE distribution to the Poisson distribution. We choose $t_z = 0.05$ and $W = 2.0$, or $L/\xi = 7.519$, and plot the level statistics in Fig. 3(c). The level statistics fits a semi-Poisson distribution $P(s) = 4se^{-2s}$ satisfactorily, which implies that the level repulsion becomes significant, even though we still have $L \gg \xi$.[36] As is expected, we find very weak, if any, dependence on system size in all the cases.

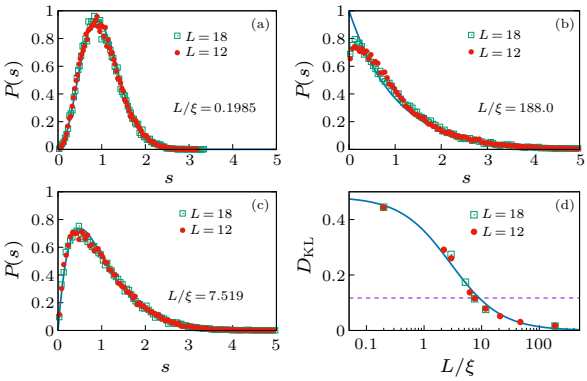

Fig. 3. Level spacing distribution of the surface states for (a) $t_z = 0.2$ and $W = 1.3$, (b) $t_z = 0.01$ and $W = 2.0$, and (c) $t_z = 0.05$ and $W = 2.0$. We compare the cubic systems of size $L = 12$ and 18. The solid lines in the plots correspond to the GUE distribution, the Poisson distribution, and the semi-Poisson distribution, respectively. (d) KL divergence of the surface-state level statistics as a function of L/ξ, with the Poisson distribution as reference. The solid line is a least-square fit of Eq. (10) to the data, and the dashed line indicates the KL divergence value for the semi-Poisson distribution.

To understand the evolution of the level-spacing distribution in the crossover regime, we evaluate the KL divergence of the level statistics. As plotted in Fig. 3(d), $D_{\rm KL}$ shows a wide crossover in L/ξ, which can be fitted by

$$D_{\rm KL} = \frac{a}{1 + bL/\xi}, \quad (10)$$

with $a = 0.482 \pm 0.014$ and $b = 0.344 \pm 0.027$. In the limit of large ξ, $D_{\rm KL}$ approaches a, which agrees with the value 0.471 for the GUE distribution. We conjecture the formula because the curve appears to be an activation function on the logarithm of L/ξ. One can think of the curve as an indicator of the metallic order of the surface states. Again, the curve exhibits no size dependence, as is expected.

The final question concerns the evolution of level statistics in the presence of increasing disorder, which closes the mobility gaps between the bands and, thus, destroys the 3D QHE.[22] Figure 4(a) plots the KL divergence of the level statistics in the energy range $1.12 < |E| < 1.53$ for two fixed $L/\xi = 2.937$ and 11.75 as a function of W in a $12 \times 12 \times 12$ system with open boundary conditions in the xy plane. The KL divergence of surface-state level statistics only depends on L/ξ, as demonstrated in Fig. 3. One would, thus, expect a constant KL divergence upon increasing W (along with t_z to maintain a fixed L/ξ). The non-monotonic change of the KL divergence in Fig. 4(a) comes from the entrance of the bulk states into the selected energy range (for surface states). For $W > 3.0$, $D_{\rm KL}$ increases in both the cases, implying that when the bulk energy gaps close as shown in Fig. 1(a), the bulk states and surface states mix significantly, hence the level statistics crosses over to metallic values in the bulk. The increase occurs regardless of the conducting nature of the surface states. Even before the

bulk gap closure, the band width increases with W and the localized states in the band tails already enters the energy range of surface states. This is reflected in the $D_{\rm KL}$ decrease with increasing disorder at $W < 3.0$, as the additional independent localized bulk states reduce the tendency of level repulsion otherwise existing among the surface states. The strong mixture of the bulk and surface states is demonstrated in Fig. 4(b), where $r_{\rm s}$ in the surface-state energy range spreads from 0 to 0.9, unlike the clear separation of the surface states in Figs. 2(a) and 2(c). The existence of the $r_{\rm s}$ peaks, albeit weak, hints that the mobility gap has not yet been closed at $W = 3.0$, which is consistent with the transfer-matrix study.[22]

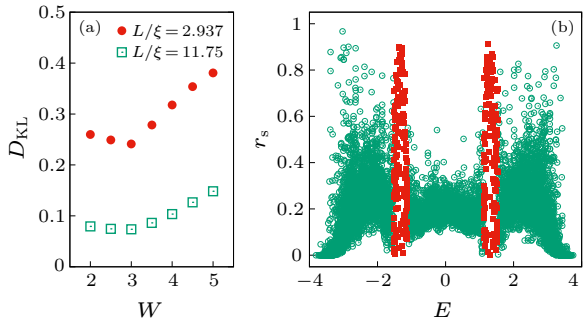

Fig. 4. (a) KL divergence of the surface-state level statistics in the energy range $1.12 < |E| < 1.53$ as a function of W for $L/\xi = 2.937$ and 11.75 in an $L = 12$ cubic system. We choose $t_z/W = 0.04$ for $L/\xi = 2.937$ and $t_z/W = 0.02$ for $L/\xi = 11.75$, respectively. (b) The surface-to-bulk $r_{\rm s}$ as a function of E in an arbitrary disorder realization with $t_z = 0.1$ and $W = 3.0$ for an $L = 21$ system. The points with $1.12 < |E| < 1.53$ are marked in red.

In summary, we explore the energy level statistics of a 3D QHE system, which supports chiral surface states in the bulk spectral gap. The surface-state level statistics crosses over from the GUE distribution, through a semi-Poisson distribution, to the Poisson distribution. We propose the use of KL divergence to quantify the evolution, which provides an order-parameter-like indicator to characterize the crossover that spans three orders of magnitude in the ratio of system size to localization length at small disorder. The mixture of the surface and bulk states under increasing disorder is characterized by a nonmonotonic KL divergence, which leads, eventually, to the collapse of the 3D QHE.

References

[1] Sarma S D and Pinczuk A 1997 *Perspectives in Quantum Hall Effects: Novel Quantum Liquids in Low-Dimensional Semiconductor Structures* (New York: Wiley)

[2] Prange R E, Cage M E, Klitzing K, Girvin S M and Chang A M 2012 *The Quantum Hall Effect* (New York: Springer)

[3] Störmer H L, Eisenstein J P, Gossard A C, Wiegmann W and Baldwin K 1986 *Phys. Rev. Lett.* **56** 85

[4] Chalker J T and Dohmen A 1995 *Phys. Rev. Lett.* **75** 4496

[5] Druist D P, Turley P J, Maranowski K D, Gwinn E G and Gossard A C 1998 *Phys. Rev. Lett.* **80** 365

[6] Liu J Y, Yu J, Ning J L, Yi H M and Miao L 2019 arXiv:1907.06318 [cond-mat.mtrl-sci]

[7] Sakai H, Fujimura H, Sakuragi S, Ochi M and Kurihara R 2020 *Phys. Rev. B* **101** 081104(R)

[8] Halperin B I 1987 *Jpn. J. Appl. Phys.* **26** 1913

[9] Tang F, Ren Y, Wang P, Zhong R and Schneeloch J 2019 *Nature* **569** 537

[10] Galeski S, Ehmcke T, Wawrzyńczak R, Lozano P and Brando M 2020 arXiv:2005.12996 [cond-mat.str-el]

[11] Qin F, Li S, Du Z Z, Wang C M and Zhang W 2020 *Phys. Rev. Lett.* **125** 206601

[12] Wang P, Ren Y, Tang F, Wang P and Hou T 2020 *Phys. Rev. B* **101** 161201(R)

[13] Galeski S, Zhao X, Wawrzyńczak R, Meng T and Förster T 2020 *Nat. Commun.* **11** 5926

[14] Cooper J R, Kang W, Auban P, Montambaux G and Jérome D 1989 *Phys. Rev. Lett.* **63** 1984

[15] Hannahs S T, Brooks J S, Kang W, Chiang L Y and Chaikin P M 1989 *Phys. Rev. Lett.* **63** 1988

[16] Hill S, Uji S, Takashita M, Terakura C and Terashima T 1998 *Phys. Rev. B* **58** 10778

[17] Kopelevich Y, Torres J H S, da S R R, Mrowka F and Kempa H 2003 *Phys. Rev. Lett.* **90** 156402

[18] Bernevig B A, Hughes T L, Raghu S and Arovas D P 2007 *Phys. Rev. Lett.* **99** 146804

[19] Cao H, Tian J, Miotkowski I, Shen T and Hu J 2012 *Phys. Rev. Lett.* **108** 216803

[20] Masuda H, Sakai H, Tokunaga M, Yamasaki Y and Miyake A 2016 *Sci. Adv.* **2** e1501117

[21] Huckestein B 1995 *Rev. Mod. Phys.* **67** 357

[22] Wang X R, Wong C Y and Xie X C 1999 *Phys. Rev. B* **59** R5277

[23] Balents L and Fisher M P A 1996 *Phys. Rev. Lett.* **76** 2782

[24] Mathur H 1997 *Phys. Rev. Lett.* **78** 2429

[25] Balents L, Fisher M P A and Zirnbauer M R 1997 *Nucl. Phys. B* **483** 601

[26] Gruzberg I A, Read N and Sachdev S 1997 *Phys. Rev. B* **55** 10593

[27] Gruzberg I A, Read N and Sachdev S 1997 *Phys. Rev. B* **56** 13218

[28] Cho S, Balents L and Fisher M P A 1997 *Phys. Rev. B* **56** 15814

[29] Plerou V and Wang Z 1998 *Phys. Rev. B* **58** 1967

[30] Kim Y B 1996 *Phys. Rev. B* **53** 16420

[31] Wang Z 1997 *Phys. Rev. Lett.* **79** 4002

[32] Chalker J T and Coddington P D 1988 *J. Phys. C* **21** 2665

[33] Kramer B, Ohtsuki T and Kettemann S 2005 *Phys. Rep.* **417** 211

[34] Zheng C, Yang K and Wan X 2020 *Phys. Rev. B* **102** 064208

[35] Efetov K B 1983 *Adv. Phys.* **32** 53

[36] Sörensen M P and Schneider T 1991 *Z. Phys. B* **82** 115

[37] Hofstetter E and Schreiber M 1993 *Phys. Rev. B* **48** 16979

[38] Shklovskii B I, Shapiro B, Sears B R, Lambrianides P and Shore H B 1993 *Phys. Rev. B* **47** 11487

[39] Zharekeshev I K, Batsch M and Kramer B 1996 *Europhys. Lett.* **34** 587

[40] Mirlin A D 2000 *Phys. Rep.* **326** 259

[41] Mehta M L 1991 *Random Matrices* (Academic, New York)

[42] Zheng C, Yang K and Wan X 2021 *Phys. Rev. B* **103** 075401